1   **Title:**

2   *Giardia colonizes and encysts in high density foci in the murine small intestine*

3

4   [¶1]NR Barash, [¶1]C Nosala, [1]JK Pham, [1]SG McInally, [2]S Gourguechon, [1]B McCarthy-Sinclair, and *[1]SC Dawson

5

6   [1]Department of Microbiology and Molecular Genetics

7   One Shields Avenue

8   UC Davis

9   Davis, CA 95616

10

11   [2]Department of Molecular and Cell Biology

12   345 LSA Bldg.

13   UC Berkeley

14   Berkeley, CA 94720

15

16   Corresponding author

17   scdawson@ucdavis.edu

18

19   [¶]These authors contributed equally to this work.

20

21

22

1

1   **Abstract**

2   *Giardia lamblia* is the most prevalent protistan parasite, causing acute and chronic diarrheal disease in over

3   one billion people worldwide. Vertebrate hosts ingest *Giardia* cysts from contaminated sources, and these

4   cysts excyst in the gut to become motile trophozoites. Trophozoites colonize the small intestine by attaching

5   to the intestinal villi and later differentiate into infectious cysts that are released into the environment,

6   completing *Giardia's* life cycle. Due to the limited accessibility of the gastrointestinal tract, our understanding

7   of *in vivo* temporal and spatial dynamics of giardiasis is largely inferred from parasite physiology in laboratory

8   culture. Yet parasite growth under *in vitro* culture conditions may not mirror *in vivo* parasite physiology in the

9   host. Here we develop bioluminescent imaging (BLI) methods to directly interrogate the temporal and spatial

10 dynamics of giardiasis in mice, providing an improved animal model for the evaluation of anti-*Giardia* drugs.

11 This non-invasive method of imaging giardiasis allows unprecedented and precise quantification of *in vivo*

12 temporal and spatial patterns of infection. By infecting mice with parasites expressing constitutive or

13 encystation-specific luciferase bioreporters, we show that parasite colonization of the gut is not uniform.

14 Metabolically active parasites primarily colonize the proximal small intestine in "hot spots"—high density foci

15 of infection that likely result in localized pathology to the gut epithelium. Using *in vivo* and *ex vivo* BLI of

16 encystation-specific bioreporters, we show that encystation initiates shortly after inoculation and parasites

17 encyst throughout the entire duration of infection. We also find that encystation is initiated in high density

18 foci in the proximal small intestine, rather than the colon as has been previously assumed, and show that the

19 initiation of encystation is magnified in parasites incubated at high density in laboratory culture. Prior models

20 have suggested that chemical cues cause parasites to encyst as they are dislodged from the upper gut and

21 travel to more distal regions of the gastrointestinal tract. We suggest a model of encystation in which

22 parasites reach a threshold density that results the induction of encystation due to local nutrient depletion.

1   The *in vivo* imaging of giardiasis has redefined the dynamics of the *Giardia* life cycle in the host, paving the

2   way for future mechanistic studies of density-dependent processes in this highly prevalent, yet understudied

3   parasite.

4

1   INTRODUCTION

2   *Giardia lamblia* is a unicellular protistan parasite causing acute and chronic diarrheal disease in over one

3   billion people worldwide, primarily in developing countries with inadequate sanitation and water treatment

4   (1, 2). Giardiasis is a serious disease of children, who may experience substantial morbidity including diarrhea,

5   malnutrition, wasting, and developmental delay (3-5). In the United States, giardiasis is the most frequently

6   diagnosed cause of water-borne diarrheal disease, and commonly affects travelers and immunosuppressed

7   individuals (6). Trophozoites are not invasive and giardiasis does not produce a florid inflammatory response;

8   however, giardiasis is associated with villus shortening, enterocyte apoptosis, hypermobility, and intestinal

9   barrier dysfunction (7). The estimated failure rates of up to 20% for standard drug treatments such as

10   metronidazole (8) and growing evidence of drug resistance in *Giardia* (9-11), underscore the need for new

11   therapeutic treatments of this widespread and neglected diarrheal disease.

12   Motile *Giardia* trophozoites colonize and proliferate in the small intestine (12), attaching to the

13   intestinal villi to resist peristalsis using a complex microtubule structure termed the ventral disc (13, 14). In the

14   gut, trophozoites differentiate into infectious cysts that are eventually excreted and can contaminate water

15   sources in the environment (6, 15). Disseminated cysts are ingested from contaminated water, and then

16   excyst into trophozoites after passage through the stomach, completing their life cycle in the host

17   gastrointestinal tract. Trophozoites are proposed to colonize the acidic, cholesterol-rich jejunum and then

18   initiate encystation when peristalsis sweeps them to the alkaline, cholesterol-depleted distal intestine (16-18).

19   Encystation is thus believed to be triggered via cues from a specific gastrointestinal anatomical site (17, 19),

20   and can be induced *in vitro* by lowering pH and cholesterol, and increasing bile and lactic acid in the medium

21   (16, 20). However, cysts produced *in vitro* are less robust at establishing infections in animal models than

1 cysts harvested directly from feces, implying that additional host factors are required for infectious cyst

2 production (17).

3   As differentiation of the trophozoite into the infectious cyst is a critical aspect of *Giardia*'s

4 pathogenesis (21), determining the extent of *in vivo* parasite differentiation to cysts and subsequent cyst

5 dissemination is key to understanding *in vivo* host-parasite interactions (22-24). Despite decades of study,

6 there remains a lack of understanding of the *in vivo* host-parasite infection dynamics underlying the extent

7 and progression of acute and chronic giardiasis (5, 25-27). Animal models of giardiasis include adult (28, 29) or

8 suckling mice (30) or adult gerbils (31) infected with either *Giardia lamblia or G. muris* isolates (32). The adult

9 mouse model of giardiasis is commonly used to evaluate anti-giardial drugs (33). Observation and

10 quantification of *in vivo* parasite physiology and differentiation has primarily been indirect, however, and *in*

11 *vivo* physiological studies are have been contingent on isolating parasites from sites of infections in animal

12 models post-sacrifice.

13   Due to the limited accessibility of the gastrointestinal tract (16-18), our understanding of the temporal

14 and spatial infection dynamics of giardiasis is largely inferred from laboratory culture rather than *in vivo*

15 models of the disease (16, 18). While *in vitro* studies have established that the initiation of encystation is

16 transcriptionally controlled (9-11), understanding the complex spatiotemporal dynamics of the parasite life

17 cycle and interactions with the host remains challenging. *In vitro* models of giardiasis are not adequate proxies

18 for infection within the host as they do not accurately mirror *in vivo* parasite physiology, and *in vitro* studies

19 rarely have been confirmed through analogous *in vivo* studies of parasite physiology. Thus, *in vivo* models are

20 necessary to understand parasite infection dynamics in the host and to evaluate new anti-giardial drugs.

21   To assess parasite colonization and differentiation dynamics in the host, we developed bioluminescent

22 imaging methods (BLI) allowing us to directly quantify and image temporal and spatial dynamics of giardiasis.

5

1   Specifically, we have infected mice with trophozoites expressing firefly luciferase under the control of

2   constitutive or encystation-specific (34-38) promoters. BLI enables sensitive quantification and live reporting

3   of transcriptional activity of protein fusions (39-41), and has been used previously to monitor parasitic

4   infection dynamics during malaria, leishmaniasis, trypanosomiasis, and toxoplasmosis (42-44), as well as

5   bacterial colonization of the intestine (34). Non-invasive imaging of bioluminescent *Giardia* parasites permits

6   unprecedented access to real-time host-parasite interactions, allowing us to revise decades-old assumptions

7   about *Giardia* infection and encystation dynamics in living hosts. Importantly, we demonstrate that

8   metabolically active parasites primarily colonize the proximal small intestine, rather than colonizing the mid-

9   jejunum as has been previously reported in adult mice (28) and immunodeficient mice (17), or inferred from

10   the identification of cysts in distal anatomical sites of the gastrointestinal tract (e.g. ileum and colon) (20, 23).

11   Further, we improve our understanding of the *in vivo Giardia* life cycle, demonstrating that encystation is

12   initiated early in the course of infection, peaks within first week, and is correlated with the highest parasite

13   density during infection. Quantification of encystation-specific vesicles (ESVs) in trophozoites colonizing the

14   proximal small intestine confirms the observations made using BLI. Lastly, we demonstrate that local parasite

15   density in the host contributes to the induction of encystation-specific transcription *in vitro* and may

16   contribute to the early *in vivo* differentiation of parasites in mice. Using BLI to evaluate *in vivo* giardiasis

17   permits precise longitudinal and spatial monitoring of the dynamics of infection, and provides an improved

18   method to evaluate anti-giardial drugs in a relevant animal model of giardiasis.

19

20   **RESULTS**

21   ***Visualizing and quantifying Giardia infection dynamics using non-invasive bioluminescent imaging***

6

1   To confirm that the promoter-firefly luciferase (FLuc) fusions are stably integrated and that the

2   bioluminescence is not lost in the absence of antibiotic selection (Supplemental Figure S1), we used *in vitro*

3   bioluminescence assays to monitor luciferase activity after the removal of antibiotic selection (Supplemental

4   Figure S2B). Both P_{GDH}-*FLuc* and P_{CWP1}-*FLuc* strains maintained a consistent bioluminescence for at least three

5   weeks under normal growth conditions (Supplemental Figure S2B). Luciferase catalyzes the production of light

6   in the presence of luciferin substrate. While oxygen is required for light production, the colon has sufficient

7   oxygen for detectible light output (45). Because *Giardia* trophozoites proliferate in the low oxygen gut lumen,

8   we tested D-luciferin delivery both orally (by gavage) and systemically (by intraperitoneal injection) to

9   determine the delivery method that produced the optimal bioluminescent signal (Supplemental Figure S3A).

10   Intraperitoneal injection caused animals less stress and produced stable bioluminescence from bioreporter

11   strains for over 30 minutes after injection (Supplemental Figure S3B). Uninfected mice or mice infected with a

12   non-luminescent strain of *Giardia* had negligible background signal (Figure 1A).

13

14

15   To query the temporal sequence of both *in vivo* colonization and encystation, we infected a cohort of mice

16   with one million P_{GDH}-*FLuc* trophozoites and quantified the bioluminescent signal over a 14-day time course

17   (Figure 1). At day 7, we observed significant bioluminescence as compared to uninfected animals (ratio paired

18   T test, p<0.0067). Individual mice showed variation in the degree of bioluminescent signal (Figure 1A) and

19   some animals exhibited signal periodicity; one representative individual (Figure 1B) showed bioluminescence

20   peaks at day 4, day 10 and day 12 post-infection. Maximum bioluminescence occurred between day 4 and day

21   9 for all animals infected with the P_{GDH}-*FLuc* strain (n=20 over two experiments, Figure 1C). To ensure the

22   bioluminescent signal was attributable to metabolically active parasites, we also treated mice infected with

1   the P_{GDH}-FLuc strain with 50 mg/kg metronidazole by oral gavage. After two days of treatment, the

2   bioluminescent signal had decreased to the same level as non-infected animals (Figure 1D).

3

4   ***Quantifying the spatial variation of giardiasis using ex vivo imaging of the gastrointestinal tract***

5   To assess spatial infection dynamics and to correlate non-invasive imaging with *ex vivo* imaging of excised

6   intestine, we inoculated twenty-one mice with one million P_{GDH}-FLuc trophozoites. On days 1, 3, 5, 7, 9, 11,

7   and 13 post-infection, three or four animals were individually imaged. Animals were then sacrificed, and the

8   gastrointestinal tracts were quickly excised and imaged *ex vivo* (Figure 2). We observed four major patterns of

9   bioluminescence within the gastrointestinal tracts over the course of infection (representative patterns are

10   shown in Figure 2A). The majority of bioluminescent signal occurred in the proximal small intestine as early as

11   one day following oral gavage (Figure 2B), yet there was some spatial variability in the gastrointestinal parasite

12   colonization pattern in the cohorts over the thirteen days. Further, we observed localized areas of maximal

13   bioluminescent signal, or foci, within colonized regions of the gut (Figure 2A). These regions are upwards of

14   100 fold more bioluminescent than adjacent regions in the same anatomical section. In some animals,

15   bioluminescence was present in the distal small intestine or diffuse throughout the small intestine. Less

16   commonly observed was bioluminescence occurring primarily in the cecum or the large intestine. For all

17   samples, BLI signal intensities of less than 1% of total maximal signal were seen within the stomach. The *in*

18   *vivo* imaging signal intensities were directly comparable with the *ex vivo* imaging (Supplemental Figure S5).

19

20   Through a comparison of colonization patterns during early, mid, and late infections (Figure 2B), we found that

21   early in infection, there was more diffuse small intestinal colonization, with 48% of the BLI signal from all

22   animals localized to the proximal small intestine and nearly one third of signal from the distal small intestine.

8

1 At maximal infection, the proximal small intestine was more strongly colonized than the distal, accounting for

2 71% of overall signal. Four of eleven mice (36%) had a proximal-only colonization pattern, with an average of

3 89% proximal signal amongst the individuals. Only one mouse had significant colonization of the distal

4 intestine. Late in infection, higher BLI signal intensity was detected in the distal small intestine and cecum,

5 although the proximal small intestine still accounted for 57% of overall signal. Early and late infections were

6 characterized by a more diffuse pattern throughout the gastrointestinal tract, whereas during the maximal

7 infection (mid infection) more parasites are concentrated in the proximal small intestine.

8 We next compared parasite quantification obtained using the BLI signal of the P_{GDH}-FLuc bioreporter

9 with other methods of parasite quantification. Following ex vivo imaging and quantification of

10 bioluminescence, we quantified total parasites using qPCR of genomic DNA isolated from one-centimeter

11 intestinal segments in regions of high and low bioluminescent signal (Supplemental Figure S4). We amplified

12 the Giardia pyruvate ferredoxin oxidoreductase gene (PFOR1) and used the constitutively expressed murine

13 nidogen-1 gene as an internal control to determine the contribution of murine DNA to total genomic DNA

14 isolated from intestinal segments. A smaller difference in differential counts to threshold (ΔCT) between

15 nidogen and PFOR indicated greater parasite as more murine DNA was present than Giardia DNA, while a

16 larger difference in ΔCT indicated fewer parasites. We determined that there is a significant and linear

17 association between bioluminescence intensity and infection density (Supplemental Figure S4, p < 0.0001).

18

19 **Encystation occurs early in infection in both the proximal and the distal small intestine**

20 Giardia cysts consist of a partially divided trophozoite surrounded by a desiccation resistant cyst wall that is

21 composed predominantly of leucine-rich cyst wall proteins (CWPs). CWPs are transported to the outer

22 membrane by encystation-specific vesicles (ESVs) approximately six hours after transfer to in vitro encystation

1   medium (23, 46). Cyst wall protein 1 (CWP1) expression is upregulated several hundred fold within seven

2   hours after switching to *in vitro* encystation medium (23) (47). The bioluminescent signal from the P_{CWP1}-*FLuc*

3   strain increased 400-fold when transferred to *in vitro* encystation medium (Supplemental Figure S2). This

4   signal intensity was maintained for over three weeks of serial passage without antibiotic selection

5   (Supplemental Figure S2B).

6   To determine the temporal and spatial dynamics of *Giardia* encystation *in vivo*, we inoculated eight

7   mice with one million P_{CWP1}-*FLuc* expressing trophozoites. P_{CWP1}-*FLuc* bioluminescence was quantified every

8   other day in live animals. One day post-infection we observed significant P_{CWP1}-*FLuc* signal (Figure 3A),

9   comparable to *in vitro* transcriptional upregulation of CWP1 (Supplemental Figure S2 and (23, 47)). The

10   maximal BLI signal from the P_{CWP1}-*FLuc* bioreporter occurred at 6 days post-infection, and significant signal

11   ranged from five to eight days post inoculation (Figure 3B). While the P_{CWP1}-*FLuc* bioluminescence from all

12   animals was highest within the first week of infection, the bioluminescence was detectable throughout the

13   17 days of infection including day 1 (early infection), day 6 (mid-infection), and day 15 (late infection) (Figure

14   3B).

15

16

17   To determine the regions of the murine gut where encystation is initiated, cohorts of three animals were

18   sacrificed on days 1, 3, 6, 10, 15, 20, and 26 post inoculation with the encystation bioreporter strain P_{CWP1}-

19   *FLuc*, and the entire GI tract was imaged and scored by region (Figure 3A). Upregulation of the P_{CWP1}-*FLuc*

20   encystation bioreporter was detectable *ex vivo* as early as day one post infection. Maximal P_{CWP1}-*FLuc*

21   bioluminescence was primarily observed in the proximal small intestine, three to five centimeters distal to

22   the stomach, similar to the constitutive P_{GDH}-*FLuc* bioreporter strain. Like P_{GDH}-*FLuc*, P_{CWP1}-*FLuc*

1   bioluminescence was often observed as regions of local maxima or foci within an area of lower

2   bioluminescence (Figure 2 and Figure 3).

3   In contrast to the P_{GDH}-FLuc bioreporter strain, bioluminescence from the encystation bioreporter

4   P_{CWP1}-FLuc was distributed throughout the entire small intestine (Figure 3A). Early in infection, equal

5   numbers of mice displayed P_{CWP1}-FLuc bioluminescence in the proximal and distal small intestines (Figure

6   3C), yet the bioluminescence from P_{CWP1}-FLuc localizing to the proximal SI accounted for 50% of total

7   intensity, whereas the distal SI signal was only 16% of the total bioluminescence in the gut. At mid and late

8   infection, proximal and distal SI signal intensities were comparable (54% and 40%, peak; 37% and 44%, late)

9   with equal numbers of mice showing signal from both proximal and distal SI regions.

10   We also noted increased localization of P_{CWP1}-FLuc bioluminescent signal to the cecum, as compared

11   to P_{GDH}-FLuc, which localized primarily to the proximal small intestine (Figure 2). Two mice from early

12   infection and one from late infection had strong cecal bioluminescent signals, sometimes at the exclusion of

13   other anatomical sites, or in conjunction with bioluminescence elsewhere in the gastrointestinal tract.

14

15   ***Confirmation of encystation initiation in the proximal small intestine during early infection***

16   To confirm the encystation initiation pattern early in infection, we infected animals with a second encystation

17   specific strain, P_{CWP2}-FLuc, containing the promoter region of the cyst wall protein 2 (CWP2) gene (48). The

18   temporal and spatial dynamics of encystation initiation we observed with P_{CWP2}-FLuc were similar to those of

19   P_{CWP1}-FLuc (Supplemental Figure S6).

20   Because infections with both encystation-specific P_{CWP1}-FLuc and P_{CWP2}-FLuc bioreporter strains

21   indicated that encystation initiation occurs early during infection and is primarily localized to the proximal SI,

22   we confirmed the expression of CWP1 transcripts throughout the gut using qPCR of *ex vivo* samples following

1   bioluminescent imaging. Within the first five centimeters of the proximal SI, transcription of CWP1 was

2   upregulated by three days post infection, with significantly more upregulation by day 7 relative to basal CWP1

3   transcription levels in *in vitro* culture (Figure 4A).

4

5   Upregulation of encystation-specific promoter activity results in the commitment of trophozoites to

6   differentiate into cysts that are shed into the environment to infect new hosts (47). Hallmarks of this

7   commitment to encystation include the upregulation of CWP1 and CWP2 genes, and the appearance of

8   encystation specific vesicles (ESVs) that transport the cyst wall proteins (e.g., CWP1 and CWP2) to build the

9   cyst wall (49, 50). We find that *in vivo* CWP1 gene expression corresponds to the *in vivo* BLI signal of the P_{CWP1}-

10   *FLuc* strain. As previously shown in Figure 3, the P_{CWP1}-*FLuc* bioluminescence is localized in foci throughout in

11   the proximal and distal small intestine (Figure 4B). We observed a significant increase in CWP1 gene

12   expression (relative to GAPDH) in these foci of the distal small intestinal and proximal small intestinal region.

13   Specifically, we quantified 8 fold and 19 fold higher CWP1 gene expression in the proximal and distal small

14   intestine, respectively, relative to GAPDH expression.

15   During *in vitro* encystation, ESVs appear within 5-7 hours following transfer to encystation medium (19,

16   47, 51). On days 3 and 7 post infection, we immunostained *ex vivo* intestinal samples using an anti-CWP1

17   antibody (50) and confirmed that trophozoites with encystation-specific vesicles (ESVs) were also present

18   throughout the small intestine (Figure 4C). CWP1 positive cells represented approximately 80% of the total

19   cells imaged in the distal small intestine (Figure 4C). Specifically we identified at least twenty ESVs in each

20   trophozoite positive fro ESVs that were isolated from the proximal regions of the small intestine (see

21   representative images, Figure 4C).

22

1   ***Increased parasite density contributes to encystation initiation***

2   *Ex vivo* spatial imaging of bioluminescence showed that trophozoite colonization of the host gut is not

3   uniform; rather, vegetative and encysting trophozoites are concentrated in foci, primarily within the proximal

4   small intestine (Figure 2, Figure 3, and Supplemental Figure S6). Localized areas of increased parasite density

5   might affect the physiology or differentiation of parasites in this particular region, perhaps contributing to

6   developmental transitions. To assess whether the observed encystation promoter activity in mice was a

7   consequence of initial concentrations of trophozoites used during gavage, we inoculated cohorts of mice (N=4

8   mice per group, n=12 total) with three different densities of P_{CWP1}-*FLuc* trophozoites (Figure 5A). P_{CWP1}-*FLuc*

9   signal intensity was dependent on inoculum density during the first 6 days post-inoculation. After day 6, the

10   bioluminescent signal reached a maximum that was similar for all three inoculum densities, with a slight and

11   gradually decline over the next two weeks (Figure 5A). Of eight mice imaged daily for 14 days, the maximum

12   bioluminescence was reached at an average of 6 days, with a range between five and eight days. With respect

13   to the spatial location of encystation, at day 21 post infection, regardless of initial inoculation density, the *ex*

14   *vivo* bioluminescent signal primarily remained in the proximal and distal small intestine (Figure 5B) although

15   some animals had distal or cecum bioluminescence. We suggest that once the initial inocula reaches a

16   colonization density threshold, perhaps localized to foci, encystation initiation occurs at the maximal level.

17   To evaluate whether parasite density had an effect on the initiation of encystation *in vitro*, we

18   "crowded" cultures of the constitutive bioreporter (P_{GDH}-*FLuc*) strain (Figure 5C) or the encystation-specific

19   bioreporter *(P_{CWP1}-FLuc)* strain (9 hours, Figure 5D) with increasing amounts of non-luminescent wild type

20   WBC6 in encystation buffer. Then we quantified bioluminescence at 3, 6, 9 and 12 hours after transfer to

21   encystation medium (9 hours, Figure 5C and 3-12 hours, Supplemental Figure S7). Within nine hours, we

22   observed a significant increase in bioluminescence from the P_{CWP1}-*FLuc* strain with the addition of 5×10^5 -2×10^6

13

1   additional trophozoites to the P_{GDH}-*FLuc* (5D) as compared to no increase in bioluminescence with crowding of

2   the P_{GDH}-*FLuc* strain (Figure 5C).

3

4   **DISCUSSION**

5   Despite its global burden, zoonotic potential, and emerging evidence of resistance to the most commonly used

6   drugs (52, 53), *Giardia's* pathogenesis in the host remains poorly understood. This dearth of information about

7   the diversity of host-parasite interactions occurring within distinct regions of the gastrointestinal tract is

8   primarily due to the lack of methods to directly and non-invasively interrogate disease progression in live

9   animal hosts. Current standard methods of quantifying giardiasis involve sacrificing animals in cohorts at

10   specific time points and determining parasite load by direct parasite counting or by *Giardia*-specific qPCR (4,

11   54). Here we have developed and used non-invasive live bioluminescence imaging of giardiasis in mice to

12   define *in vivo* spatiotemporal patterns of parasitic colonization and differentiation.

13

14   **Non-invasive quantification of *in vivo* temporal dynamics of giardiasis**

15   Unraveling the complex relationship between host and parasite requires use of an *in vivo* model of infection.

16   The most widely used animal model of giardiasis is infection of mice with human disease-associated *Giardia*

17   strains (WB or GS) (28). Parasite burden in mice has been most commonly quantified by directly counting

18   trophozoites in short segments of duodenum or jejunum, or more recently, by *Giardia*-specific qPCR (4, 54).

19   Directly counting trophozoites in 2-3 cm segments of small intestine is laborious and subject to sampling

20   errors. In live animals, quantification of fecal cysts is commonly used to estimate parasite abundance, yet cyst

21   shedding may be a poor surrogate for overall parasite burden (55). Overall, bioluminescence imaging provides

22   a faster and more sensitive evaluation of parasite burden than the current gold standard for parasite

1 enumeration (56).

2 Non-invasive *in vivo* BLI relies on the external detection of light produced internally, and signal

3 intensity may be limited by the overall level of luciferase expression, the oxygen tension within relevant

4 tissues, pigmentation of organs and skin, or any background signal from the animal (35). However, the gut is

5 sufficiently oxygenated to permit signal detection, and while animal tissues exhibit relatively high background

6 levels of autofluorescence, they have nearly nonexistent levels of autoluminescence, which facilitates

7 detection even at low signal strength (35, 37, 57). We monitored and quantified *in vivo* expression of

8 metabolic and encystation genes for up to three weeks using cohorts of mice infected with one of three

9 *Giardia* bioluminescent reporter strains (P_{GDH}-*FLuc,* P_{CWP1}-*FLuc* or P_{CWP2}-*FLuc)*. Using the constitutively

10 expressed P_{GDH}-*FLuc* strain, we confirmed maximal infection at approximately seven days, consistent with

11 prior studies of giardiasis in mice (28). This live imaging strategy provides the first real-time visualization of the

12 spatial and temporal dynamics of giardiasis *in vivo*, allowing us to assess the timing and location of parasite

13 differentiation. Cysts are known to be shed sporadically and sometimes cyclically (58, 59). Similar to the

14 variability in human giardiasis (60), we also observed variability in infections between isogenic cage mates,

15 including variations in the time to maximum infection, spatial colonization patterns, and cyclical infections

16 (Figures 1-3). We confirmed that infection dynamics change based on the number of parasites inoculated, but

17 that as a whole and as previously reported, parasite burdens peaks at about one week after infection.

18

19 **Reassessing the spatial dynamics of giardiasis in the mouse model**

20 The convoluted route of the animal gut and the diffusion and refraction of bioluminescence presents a

21 challenge when imaging giardiasis in live animals (34). Differentiating localized parasite activity from diffuse

22 infection using *in vivo* optical imaging is also challenging (Fig 1 and 2). To resolve the spatial dynamics of *in*

15

1   *vivo* infection, we used e*x vivo* imaging of bioreporters of both metabolic activity and encystation. Based on

2   early studies using direct counting of trophozoites from intestinal samples, *Giardia* has generally been

3   assumed to primarily colonize the mid-jejunum, or middle section of the small intestine (17, 61, 62), although

4   other early work suggested that trophozoites prefer to colonize throughout the proximal small intestine (17).

5   Rather than uniformly colonizing throughout a region of the GI tract, we show that *Giardia* colonizes the

6   intestine with a non-uniform or patchy distribution, characterized by discrete foci of colonization (Figure 2),

7   while encystation initiation also occurs in discrete foci within the proximal and distal small intestine, or

8   occasionally the cecum (Figure 3 and Supplemental Figure 5).

9   These high-density foci of infection are also upregulated in encystation initiation. Using *ex vivo* BLI, we

10   imaged discrete foci of encysting trophozoites in the proximal small intestine and not other anatomical sites

11   such as the cecum or large intestine. These observations challenge conventional assumptions that chemical

12   cues in the distal gut are solely responsible for the initiation of *in vivo* trophozoite differentiation to the cyst in

13   the *Giardia* life cycle. We found that metabolically active trophozoites are predominantly located in the

14   proximal small intestine, with areas of local intensity frequently just distal to the pylorus (Figures 2 and 3). We

15   also observed spatial variability between individuals, from diffuse infection throughout the small intestine to

16   patchy foci only in the distal small intestine or cecum. Maximal bioluminescence (and thus infection)

17   correlated strongly with proximal small intestinal colonization, whereas developing or clearing infections were

18   present more diffusely throughout the gastrointestinal tract (Figure 3).

19

20   **High-density foci of parasites contribute to encystation initiation**

21   The prevailing view of trophozoite differentiation to cysts in the host has been extrapolated from the

22   chemistry of the region gut where trophozoites were believed to encyst (16-18). Parasite commitment to

1   encystation and excystation are key events in *Giardia*'s life cycle, and it is clear that these transitions are highly

2   regulated (47). Premature or tardy encystation can limit cyst development, proliferation, transmission into the

3   environment, and dissemination to new hosts (55). The transition to the cyst form begins with detection of

4   encystation stimuli, resulting in transcriptional upregulation of encystation-specific cyst wall proteins (CWPs)

5   (23, 46). Almost 30 years ago, Gillin et al. showed that elevated bile concentrations, perhaps reminiscent of

6   the distal small intestinal environment, could induce encystation in *in vitro* culture (20, 61). When these *in*

7   *vitro* encystation protocols are used, CWPs are transported to the outer membrane via encystation-specific

8   vesicles (ESVs) within roughly six hours of exposure to encystation stimuli (23, 46). However, differentiation to

9   cysts can be induced even in the absence of bile, and several *in vitro* culture protocols have been developed to

10   induce encystation by modifying pH, bile, lactic acid, and lipid concentrations in culture (18, 23). Importantly,

11   no *in vitro* encystation protocol produces a high abundance of infectious cysts, suggesting that *in vivo*

12   encystation may not accurately recapitulate differentiation *in vivo*.

13   Our quantitative *in vivo* imaging of temporal and spatial dynamics of parasite proliferation and

14   encystation implies that there could be other factors contributing to *Giardia*'s developmental transitions

15   during its life cycle in the host. Rather than encystation uniformly occurring throughout a particular region of

16   the gut, we observed non-uniform foci of bioluminescence in infections with CWP1 and CWP2 strains (Figure 3

17   and Supplemental Figure 5). We also detected significant expression of CWP1 in *ex vivo* samples associated

18   with increased bioluminescence in both the proximal and distal small intestine (Figure 4B). Lastly, we

19   confirmed the presence of ESVs in trophozoites isolated from the proximal and distal small intestine (Figure 4),

20   indicating that encystation is initiated and proceeds normally in these regions. In contrast with prior studies,

21   this initiation of encystation occurred early in infections in the proximal small intestine (Figure 3) and peaked

22   within the same time as maximal parasite density observed using the constitutively expressing bioreporter

17

1   strain (Figure 1). While there was initial variation in the encystation bioluminescent signal proportional to the

2   amount of initial inoculum, we saw that the encystation-specific BLI signal peaked about seven days and

3   encystation BLI signal persisted throughout the twenty-one days of infection for all inoculum densities

4   (Figure4A).

5   Pathogens have evolved to take advantage of the discrete mucosal surfaces and functions associated

6   with the various anatomical regions of the mammalian gut (63). Reaching a particular threshold of cell density

7   is known to either directly or indirectly modulate developmental programs in diverse parasitic (64-66) and

8   free-living eukaryotes (67). Density-dependent quorum sensing is key to slender to stumpy differentiation in

9   trypanosomes, for example, and trypanosomes can also respond to or affect bacterial quorum sensing signals

10   (65, 66). Parasites such as *Giardia* detect and respond to a variety of chemical and environmental cues during

11   their life cycles, and *Giardia* has been shown to respond to alterations in lipid and pH concentrations *in vitro*,

12   triggering encystation.

13   We provide evidence that supports a model of a parasite density-based threshold for the induction of

14   encystation in the proximal small intestine and in *in vitro* culture (Figure 5). In both our *in vivo* model of

15   infection and *in vitro* culture experiments, the local parasite density of *Giardia* trophozoites may indirectly

16   induce encystation. Compared to regions colonized with a lower parasite density, intestinal regions with

17   higher parasite colonization density (foci), could directly impact the local chemistry of the gut, while indirectly

18   impacting parasite physiology, the local gut microbiome, or the host epithelium (Figure 2). With respect to

19   encystation initiation, foci of high parasite density could affect local concentrations of nutrients, metabolites,

20   and pH -- all of which are reported stimuli for encystation initiation (47). Thus we suggest that the non-

21   uniform foci of encystation-specific bioluminescence (Figure 3) represent "hotspots" of encystation in the gut.

22   Regardless of the initial number of trophozoites in the inoculum (Figure 5A) or the time post-infection (Figure

1   3), once the local density of trophozoites surpasses a specific threshold, encystation could be initiated. This

2   model of localized parasite density-induced encystation due to the depletion of nutrients or accumulation of

3   waste products is not incongruent with observed *in vitro* contributions of pH and/or lipid starvation to

4   encystation initiation (16-18).

5   Throughout the gut, high density foci of parasites could create local changes in gut chemistry that

6   could influence parasite metabolism and differentiation. In *Giardia*, the encystation signal could be induced

7   either indirectly via localized nutrient deprivation and/or accumulation of waste products, or directly via an

8   unrecognized quorum sensing-type mechanism for evaluating local cell density. Once trophozoites are

9   committed to differentiation (47) in these localized foci within the gut, later developmental stages of

10   encystation could occur more distally in the small intestine due to passage of encysting trophozoites through

11   the gastrointestinal tract, resulting in the observed accumulation and/or shedding of cysts in the lower gut.

12   While we observe some initiation of encystation within the first day of infection (Figure 3), the overall process

13   of encystation in the host is lengthy, and it may take hours before mature, infectious cysts are observed in the

14   large intestine or are recovered in feces. Further characterization of parasite physiology and differentiation in

15   high density foci as compared to low density regions of colonization will help to elucidate the contribution of

16   parasite density to *Giardia*'s developmental transitions.

17

18   **A new tool for evaluating chronic giardiasis and anti-giardial drug screening**

19   Human giardiasis typically resolves within a few weeks, yet chronic or variable infections can occur (33) and

20   have been linked to impaired physical and cognitive development in children (7). Chronic animal giardiasis

21   models have not been possible because longitudinal analyses of infection dynamics in the same animal have

22   not previously been feasible. *In vivo* BLI offers real-time and longitudinal monitoring of the infection dynamics

1   of giardiasis, providing an animal model for long-term monitoring of giardiasis in cohorts of infected animals.

2   In addition, animal numbers can be reduced with longitudinal BLI of giardiasis – a primary goal of ethical

3   animal use in research (35, 68). Dual or triple spectra bioreporter strains (69-71) could be used to

4   simultaneously assay two or more cellular processes (e.g., metabolic activity and encystation), integrating

5   different components of infection into a single study animal over time.

6   Growing evidence of drug resistance in *Giardia* underscores the need to develop new therapeutic

7   alternatives for the treatment of giardiasis (33), and *in vivo* bioluminescence imaging of murine giardiasis will

8   aid in the evaluation of promising anti-giardial drug candidates. As we have shown, BLI of luciferase-expressing

9   strains not only facilitates monitoring of parasite burden, but can also provide real-time information on other

10   aspects of parasite physiology and metabolism. We have validated the use of BLI for the analysis of anti-

11   *Giardia* drugs by demonstrating that metronidazole, the standard of care anti-*Giardia* drug that targets

12   parasite metabolic activity (72), reduced *in vivo* bioluminescence of the constitutively-expressing P_{GDH}-*FLuc*

13   bioreporter strain. Other bioluminescent reporter strains could be utilized for high-throughput *in vitro* screens

14   of candidate drugs, prior to *in vivo* assessment in mice. BLI imaging studies with anti-*Giardia* drugs targeting

15   non-metabolic parasitic cellular processes (e.g., motility or encystation) could identify adjunct or

16   complementary treatments that reduce parasite proliferation, infection duration, or cyst dissemination.

17

18   **Materials and Methods**

19   *Luciferase strain construction and validation*

20   We created two strains of *Giardia lamblia* WBC6, each with firefly luciferase (FLuc) driven by a specific *Giardia*

21   gene promoter (Supplemental Figure 1). FLuc promoter fusion constructs were integrated into the genome as

22   previously described (38). To quantify colonization and metabolic activity, we integrated a construct

1   containing FLuc driven by the constitutive NADP-specific glutamate dehydrogenase (GiardiaDB

2   GL50803_21942) promoter (P_{GDH}-FLuc) (Figure S1A). To quantify *in vivo* encystation dynamics, we integrated a

3   construct containing FLuc with the encystation-specific cyst wall protein 1 (GiardiaDB GL50803_5638)

4   promoter (P_{CWP1}-FLuc) and the encystation-specific cyst wall protein 2 (GiardiaDB GL50803_5435) promoter

5   (P_{CWP2}-FLuc) (Figure S1B and S1C). Briefly, a vector previously used to integrate HA-tagged aurora kinase (73)

6   was modified to contain the coding sequence for firefly luciferase fused to the GDH, CWP1, or CWP2

7   promoters. Puromycin (PurR) and ampicillin (AmpR) resistance cassettes allowed selection in *Giardia* and *E.*

8   *coli*, respectively. The vector was linearized using *Mlu*I and 10 μg of DNA was electroporated into *Giardia*

9   *lamblia* strain WBC6 (38). Transfected cells were selected for seven to ten days using puromycin (50 μg/ml).

10   Confirmation of successful genomic integration was obtained by PCR amplification (data not shown), as well as

11   *in vitro* bioluminescence assays in vegetative cells (*P_{GDH}-FLuc)* and encysting strains (*P_{CWP1}-Fluc and P_{CWP2}-FLuc)*

12   (Supplemental Figure S2).

13

14   *Giardia trophozoite and encystation culture conditions*

15   *G. lamblia* (ATCC 50803) WBC6, *P_{GDH}-FLuc, P_{CWP1}-FLuc,* and *P $_{CWP2}$-FLuc* strains were cultured in modified TYI-S-

16   33 medium supplemented with bovine bile and 5% adult and 5% fetal bovine serum [56] in sterile 16 ml screw-

17   capped disposable tubes (BD Falcon), and incubated upright at 37°C without shaking. Encystation was induced

18   *in vitro* by decanting TYI-S-33 medium from 24 hour cultures (roughly 30% confluent) and replacing with

19   encystation medium modified by the addition of 0.5 grams/liter bovine bile, pH 7.8 (47). After 24 hours, cysts

20   settled at the bottom of the tube.

21

22   *Giardia in vitro bioluminescence and density dependence assay*

1   To assess the stability of luciferase signal in integrated promoter-FLuc strains without selection, luciferase

2   expression in the P_{GDH}-FLuc and P_{CWP1}-FLuc strains was determined before and after passage of the cells in the

3   absence of antibiotic selection (1:25 dilutions daily for three weeks). Confluent tubes were incubated on ice

4   for 15 minutes to fully detach cells. Cells were pelleted by centrifugation at 900 x g for 5 minutes and

5   resuspended in 1 mL of fresh TYI-S-33 media supplemented with 150 µg/mL D-Luciferin (PerkinElmer).

6   Aliquots (50 µl, three technical replicates) were added to white opaque 96-well microplates (Perkin Elmer).

7   Bioluminescence was analyzed on a Victor3 plate reader using one-second exposures until maximum signal

8   was achieved.

9   For density dependence assays, wild-type and P_{CWP1}-FLuc cells were grown to confluence, harvested as

10   described, and washed and resuspended in encystation media. One hundred thousand P_{CWP1}-FLuc cells were

11   plated in each well of a microplate and a range of dilutions of non-bioluminescent wild-type WBC6 were

12   added to the P_{CWP1}-FLuc cells in three technical replicates. Encystation medium was then added to adjust the

13   final volume to 200 µL per well. Microplates were individually sealed in Type A Bio-Bags (BD) to maintain an

14   anoxic environment and incubated at 37°C for the indicated time points. D-luciferin was added to 150 µg/mL

15   and luciferase activity was analyzed as described previously.

16

17   *Non-invasive in vivo bioluminescent imaging of Giardia colonization and encystation*

18   Eight week old, female C57/B6/J mice (Jackson Laboratories) were maintained on *ad libitum* water and

19   alfalfa-free irradiated rodent pellets (Teklad 2918). To promote parasite colonization, water was

20   supplemented with 1 mg/ml ampicillin and neomycin (Teknova) for five days prior to infection (54). Water

21   bottles were kept protected from light to minimize degradation of the antibiotics and antibiotics were

22   refreshed every other day. Individual mice were marked with ear tags or permanent marker on tails, and hair

1   was removed from the ventral abdomen to facilitate imaging. Each mouse was first shaved using a

2   commercial men's groomer, and then depilatory cream (Nair) was applied for 30 seconds. For long-term

3   studies, depilatory cream was re-applied as necessary to maintain a hairless ventrum (34). Each animal was

4   gavaged with 1 x 10^7 G. lamblia trophozoites in 100 µL phosphate-buffered saline as previously described (74).

5   All animal studies were performed with IACUC approval at the University of California Davis (Scott C. Dawson,

6   PI).

7   For in vivo BLI, mice were sedated using isoflurane (1.5-3%) in an induction chamber. D-luciferin (30

8   mg/kg) was then injected intraperitoneally at a dose of 150 mg/kg body weight (total volume injected, 100

9   µL). Sedated mice were transferred to an optically clear XIC-3 Isolation Chamber (PerkinElmer) and positioned

10 on their dorsal surface. Bioluminescence was imaged using an IVIS Spectrum (PerkinElmer) with no emission

11 filter. Anesthesia was maintained with 1.5-2% isoflurane and 100% oxygen during imaging.

12   Photons were quantified using an ultra-sensitive CCD camera (IVIS Spectrum) and the resulting heat

13 maps of bioluminescent photon emission intensity were overlaid on still images of anaesthetized animals. To

14 allow the D-luciferin to distribute throughout the body, images were collected with two-minute exposures

15 constantly over 8-10 minutes until the bioluminescent signal stabilized. The final image collection was

16 performed with two to five minute exposures, dependent on signal strength. ROI analysis was used to

17 quantify bioluminescence (LivingImage). A rectangle encompassing the entire abdomen was drawn for each

18 mouse from front paws to anus. BLI data was quantified as total flux (photons/second) for exposure time-

19 independent quantification of signal intensity. For mice infected with P_{GDH}-FLuc, the minimal signal was

20 normalized to the level of background signal in uninfected mice (1x10^4 photons/sec). Because the

21 bioluminescent signal intensity from P_{CWP1}-FLuc was several orders of magnitude stronger than for mice

23

1   infected with for P_{GDH}-*FLuc*, the minimal threshold signal was adjusted to 5x10^5 photons/sec in order to

2   minimize background.

3

4   *Ex vivo bioluminescence imaging*

5   Sedated mice were euthanized by cervical dislocation. The gastrointestinal tract was quickly dissected from

6   esophagus to anus and positioned within a plastic Petri dish. The dish and contents were placed within the

7   XIC-3 Isolation Chamber, 2.5% oxygen was provided to maximize signal, and the GI tract was imaged with a

8   two-minute exposure. *Ex vivo* imaging was performed less than 30 minutes after the initial injection of

9   luciferin. ROI analysis was used to quantify bioluminescence (LivingImage). Total gastrointestinal tract signal

10   was analyzed with a circle over the entirety of the petri dish. The stomach, proximal SI (first half), distal SI

11   (second half), cecum, and large intestine were traced using the free-hand tool.

12

13   *Estimation of parasite density using quantitative PCR (qPCR)*

14   One-centimeter segments from a region showing strong *ex vivo* signal were identified, marked in the

15   LivingImage software, excised, and flash frozen in liquid nitrogen. Total genomic DNA was extracted using

16   standard methods (75), and diluted to 10 ng/μL in nuclease-free water prior to qPCR. Quantitative PCR of the

17   pyruvate-ferredoxin oxidoreductase-1 (*pfor1*, GiardiaDB GL50803_17063) gene (72) was performed using

18   Pfor1F 5'TTCCTCGAAGATCAAGTTCCGCGT3' and Pfor1R 5'TGCCCTGGGTGAACTGAAGAGAAT3' oligonucleotide

19   primers and SensiFast No-ROX cyber-green master mix in an MJ Opticon thermal cycler, with an initial 2

20   minute denaturation step at 95°C followed by 40 cycles of 95 °C for 5 seconds, 60°C for 10, and 72 °C for 10.

21   The single copy, constitutively expressed murine nidogen-1 (*nid1*) gene was used as an internal control to

22   quantify the contribution of murine DNA to intestinal segments (qPCR primers nidoF

1 5'CCAGCCACAGAATACCATCC3', nidoR 5'GGACATACTCTGCTGCCATC3'). The differential counts to threshold

2 (ΔCT) between *nid1* and *pfor1* were quantified, and Ct values were determined using the Opticon Monitor

3 software.

4

5 *Confirmation of encystation in the proximal small intestine during early infection using quantitative PCR (qPCR)*

6 A cohort of four mice was infected with P_{CWP1}-*FLuc* and two mice were imaged and sacrificed for sample

7 collection at both day 3 and day 7 p.i. Following *ex vivo* imaging, intestines from infected mice were dissected

8 into 3 cm segments, immediately frozen in liquid nitrogen and transferred to a -80°C freezer until used for

9 RNA extraction. RNA from intestinal segments was purified using RNA Stat-60 (Tel-test, Inc.). RNA quality was

10 assessed using spectrophotometric analysis (NanoDrop Technologies) and electrophoresis prior to cDNA

11 synthesis. Double-stranded cDNA was synthesized using the QuantiTect Reverse Transcription Kit (Qiagen).

12 Quantitative PCR of cyst wall protein 1 (CWP1, GiardiaDB GL50803_5638) was performed using cwp1F

13 5'TAGGCTGCTTCCCACTTTTGAG 3' and cwp1R 5'AGGTGGAGCTCCTTGAGAAATTG 3'oligonucleotide primers

14 (76)and SensiFast No-ROX cyber-green master mix in an MJ Opticon thermal cycler, with an initial two minute

15 denaturation step at 95°C followed by 40 cycles of 95 °C for 5 seconds, 60°C for 10 s, and 72 °C for 10 s. The

16 constitutively expressed gene for glyceraldehyde 3-phosphate dehydrogenase (GAPDH, GiardiaDB GL50803_

17 6687) was chosen as an internal reference gene and was amplified with gapdh-F 5' CCCTTCACGGACTGTGAGTA

18 3' and gapdh-R 5' ATCTCCTCGGGCTTCATAGA 3' oligonucleotide primers. Ct values were determined using the

19 Opticon Monitor software and statistical analyses were conducted using Prism (GraphPad).

20

21 *Immunostaining of encysting trophozoites in intestinal tissue samples*

25

1   Intestinal segments from the same infected mice analyzed with qPCR (above) were transferred to chilled

2   *Giardia* medium, incubated at 4°C for 15 minutes to allow parasite detachment, then briefly vortexed. Cells

3   remaining in the supernatant were pelleted at 900 x g for 2 minutes at 4°C, and resuspended in 0.5 ml of

4   chilled medium. Parasites were then spread on pre-warmed (37°C) glass coverslips and incubated 30 minutes

5   in a humidifying chamber to facilitate attachment. Two ml of warmed fixation buffer (4% paraformaldehyde,

6   1% glutaraldehyde in 0.86X HEPES buffered saline) was added to each coverslip and incubated at room

7   temperature for 15 minutes. Coverslips were washed three times with 2 ml of PEM buffer, and then

8   incubated in quenching buffer (0.11 M glycine in 0.9X PEM) for 15 minutes at room temperature.

9   Immunostaining was performed as previously described (77) with a mouse primary antibody against cyst wall

10   protein 1 (Giardi-a-Glo, Waterborne, Inc.) and a donkey anti-mouse secondary antibody conjugated to an

11   Alexa 350 fluorophore (Invitrogen).

12   Images were acquired via automated Metamorph image acquisition software (MDS Technologies)

13   using a Leica DMI 6000 wide-field inverted fluorescence microscope with a PlanApo 100X, NA 1.40 oil

14   immersion objective. At least 100 trophozoites were counted per slide and cells were binned into encysting or

15   normal trophozoite morphologies. Regions of small intestine were distinguished spatially as follows: proximal

16   1-4 cm, proximal 5-16 cm, and distal 17-32 cm. Slides from 3-6 separate intestinal segments were counted per

17   spatial bin. The statistical significance of differences in cell number between the spatial bins was determined

18   via Student's T-Test.

19

20   **ACKNOWLEDGEMENTS**

3

1 **Figure 1. *Bioluminescent imaging allows non-invasive quantification of Giardia infection dynamics in***

2 ***individual cohorts of mice.*** In panel A, a cohort of four of mice were inoculated with the P_{GDH}-*FLuc* strain and

3 bioluminescence at seven days post-inoculation was compared to the background signal from uninfected

4 animals (images left). P_{GDH}-*FLuc* bioluminescence intensity is indicated in the image overlays, with the highest

5 signal intensity shown in red and the lowest in blue. Bioluminescence flux (photons/second) is compared

6 between the uninfected and infected group, with the double asterisk indicating significance as assessed by the

7 ratio paired T test (p<0.0067). In B, cyclic variability of the P_{GDH}-*FLuc* bioluminescence is shown in the same

8 animal imaged non-invasively each day for fourteen days post infection. Infection dynamics in two

9 experiments with 8 and 12 mice as quantified by P_{GDH}-*FLuc* bioluminescence is summarized in panel C. The

10 average bioluminescence measured for the cohort each day is shown. The shaded box indicates the maximal

11 bioluminescent signal, or peak infection range. The average time to maximal bioluminescence after infection

12 with the P_{GDH}-*FLuc* was 6.6 days. Lastly, in D, a cohort of four mice was imaged and flux (p/s) was quantified

13 five days after infection with the P_{GDH}-*FLuc* strain (Before). The same four mice were imaged and flux was

14 quantified two days after treatment with 50 mg/kg metronidazole by oral gavage (After).

15

16 **Figure 2. *High-density foci of Giardia colonization are present in the proximal small intestine.*** Representative

17 classes of *in vivo* and *ex vivo* bioluminescent images are shown for twenty-four mice infected with the P_{GDH}-

18 *FLuc* strain and sacrificed in cohorts of four on days 3, 5, 7, 9, 11, and 13 post-infection (A). Photon flux or

19 radiance (p/s/cm^2/sr) for each intestinal segment is shown and has been normalized to the maximal *ex vivo*

20 bioluminescence signal on the radiance scale, yielding the percent total signal per segment. These values are

21 represented graphically on the gray scale maps below each *ex vivo* image (clear = 0-10% and black = 75-100%,

22 with values between 10% and 75% indicated as shades of gray). A strike through indicates greater than 90% of

23 maximal bioluminescent signal. In (B), quantitative bioluminescence imaging from infections is categorized

28

1   and summarized by the region of the gastrointestinal tract (P = proximal small intestine, D = distal small

2   intestine, C = cecum, and L = large intestine) for all animals in each phase of infection as **early** (days 0-3), **peak**

3   (days 5-9), and **late** (days 11-13). The stomach (S= stomach) is shown for orientation but always lacks

4   bioluminescence. Shading in each row of the charts indicates the variations in the maximal bioluminescence in

5   each of the four regions in an individual animal.

6

7   **Figure 3. *Encystation initiation occurs early in infection in both the proximal and distal small intestine***

8   Eighteen mice were inoculated with P_{CWP1}-*FLuc* strain, and cohorts of three animals were sacrificed and

9   imaged on days 1, 3, 6, 10, 15, and 20 post-infection. In (A), the whole animal *in vivo* images from Days 1, 6,

10   and 15, representing early, mid and late infection, are shown with corresponding *ex vivo* images from each

11   animal (S = stomach, P = proximal, D = distal, C = cecum, and L = large intestine). Days 1 and 15 are presented

12   on a scale between $1e^4$ and $1e^6$ photons/sec. Day 6 has the maximal signal, and images are presented using a

13   scale between $5e^5$ and $5e^7$ photons/sec.   For each *ex vivo* image, the photon flux (p/s/cm^2/sr) for each

14   intestinal segment is normalized to the maximal *ex vivo* bioluminescence signal on the radiance scale, yielding

15   the percent total signal per segment. Gray scale maps of bioluminescence are shown below each *ex vivo* image

16   (clear = 0-10% and black = 75-100%, with values between 10% and 75% indicated as shades of gray).   In (B),

17   two cages of mice (N=4 per cage) were inoculated with the P_{CWP1}-*FLuc* strain and imaged every other day. The

18   box plot summarizes bioluminescent signal for encystation initiation (P_{CWP1}-*FLuc)* for each phase of infection

19   (**early,** days 0-3; **mid**, days 4-9; and **late**, days 10-20). The bioluminescence from each cohort of animals is

20   categorized by the gastrointestinal region, and the overall spatial localization of signal is summarized for each

21   individual animal in each row of panel C. The shaded charts summarize the percentage of maximal

22   bioluminescent signal from the P_{CWP1}-*FLuc* strain in each of the four gastrointestinal regions (P = proximal

23   small intestine, D = distal small intestine, C = cecum, and L = large intestine) for all infected animals in early,

1   mid, and late stages of infection. The stomach (S = stomach) is shown for orientation but always lacks

2   bioluminescence.

3

4   **Figure 4. *CWP1 qPCR and immunostaining of ESVs verify encystation in the proximal and distal small***

5   ***intestine.*** Quantitative PCR was used to compare the *in vivo* expression of CWP1 relative to GAPDH

6   (CWP1/GAPDH) in the first five centimeters of the small intestine at day 3 and 7 p.i. to that of a confluent *in*

7   *vitro* culture (A). Asterisks indicate statistical significance using unpaired T tests with Welch's correction; one

8   asterisk = p < 0.05 and two asterisks = p < 0.005. In B, a representative animal infected with the P_{CWP1}-*FLuc*

9   strain is imaged non-invasively at day 7 p.i., and *ex vivo* BLI of the gastrointestinal tract (P = proximal small

10   intestine, D = distal small intestine, C = cecum, and L = large intestine) is shown with corresponding

11   CWP1/GAPDH qPCR of representative proximal and distal small intestine regions (boxed). In C, encystation

12   specific vesicles (ESV) were immunostained using an α-CWP1 antibody and quantified in pooled *ex vivo*

13   samples from two animals each at day 3 and 7 p.i. ESVs are marked by arrows in representative images from

14   each respective intestinal sample. The percentages of trophozoites positive for ESVs are shown as a

15   percentage of total trophozoites imaged (N>600 cells counted) in regions of the proximal small intestine (pSI)

16   and distal small intestine (dSI).

17

18   **Figure 5. Increased cell density contributes to encystation initiation and upregulation of CWP1 expression.**

19   To assess the impact of cell density on the initiation of encystation, cohorts of three mice were infected with

20   three different concentrations of P_{CWP1}-*FLuc* parasites (80, 8000, or 800000) and bioluminescence was imaged

21   and quantified daily over 21 days in total (A). In panel B, *in vivo* and *ex vivo* BLI is presented following sacrifice

22   at day 21. The shaded charts in B summarize the percentage of maximal bioluminescent signal from the P_{CWP1}-

23   *FLuc* strain in each of the four gastrointestinal regions (P = proximal small intestine, D = distal small intestine, C

1   = cecum, and L = large intestine) for each individual animal infected with that initial inoculum. The stomach (S

2   = stomach) is shown for orientation but always lacks bioluminescence.

3   In panels C and D, bioluminescence is quantified from an experiment in which 100,000 bioluminescent P_{GDH}-

4   *FLuc* (C) or P_{CWP1}-*FLuc* (D) trophozoites were incubated up to twelve hours in encystation medium, and each

5   well was crowded with increasing amounts (darker shaded dots) of non-bioluminescent WBC6 parasites (see

6   Methods). The nine-hour time point is shown for both strains; additional time points are presented in

7   Supplemental Figure S7. A single asterisk indicates $p < 0.05$ and a double asterisk indicates $p < 0.01$.

8

1   **References**

2

3   1.   Savioli L, Smith H, & Thompson A (2006) *Giardia* and *Cryptosporidium* join the 'Neglected

4   Diseases Initiative'. *Trends Parasitol* 22(5):203-208.

5   2.   Troeger H, *et al.* (2007) Effect of chronic Giardia lamblia infection on epithelial transport and

6   barrier function in human duodenum. *Gut* 56(3):328-335.

7   3.   DuPont HL (2013) Giardia: both a harmless commensal and a devastating pathogen. *The Journal*

8   *of clinical investigation* 123(6):2352-2354.

9   4.   Bartelt LA, *et al.* (2013) Persistent G. lamblia impairs growth in a murine malnutrition model.

10   *The Journal of clinical investigation* 123(6):2672-2684.

11   5.   Solaymani-Mohammadi S & Singer SM (2010) Giardia duodenalis: the double-edged sword of

12   immune responses in giardiasis. *Exp Parasitol* 126(3):292-297.

13   6.   Adam RD (2001) Biology of *Giardia lamblia*. *Clin. Microbiol. Rev.* 14(3):447-475.

14   7.   Halliez MC & Buret AG (2013) Extra-intestinal and long term consequences of Giardia

15   duodenalis infections. *World journal of gastroenterology : WJG* 19(47):8974-8985.

16   8.   Upcroft P & Upcroft JA (2001) Drug targets and mechanisms of resistance in the anaerobic

17   protozoa. *Clinical microbiology reviews* 14(1):150-164.

18   9.   Land KM & Johnson PJ (1999) Molecular basis of metronidazole resistance in pathogenic

19   bacteria and protozoa. *Drug Resist Updat* 2(5):289-294.

20   10.   Barat LM & Bloland PB (1997) Drug resistance among malaria and other parasites. *Infect Dis Clin*

21   *North Am* 11(4):969-987.

1   11.   Upcroft J, Samarawickrema N, Brown D, & Upcroft P (1996) Mechanisms of metronidazole

2   resistance in *Giardia* and *Entamoeba*. *Abstracts of the Interscience Conference on Antimicrobial*

3   *Agents and Chemotherapy* 36(0):47.

4   12.   Dawson SC & House SA (2010) Life with eight flagella: flagellar assembly and division in *Giardia*.

5   *Current opinion in microbiology* 13(4):480-490.

6   13.   Nosala C & Dawson SC (2015) The Critical Role of the Cytoskeleton in the Pathogenesis of

7   Giardia. *Curr Clin Microbiol Rep* 2(4):155-162.

8   14.   Elmendorf HG, Dawson SC, & McCaffery JM (2003) The cytoskeleton of *Giardia lamblia*. *Int J*

9   *Parasitol* 33(1):3-28.

10   15.   Gillin FD, Reiner DS, & McCaffery JM (1996) Cell biology of the primitive eukaryote *Giardia*

11   *lamblia*. *Annu Rev Microbiol* 50:679-705.

12   16.   Lujan HD, Mowatt MR, Byrd LG, & Nash TE (1996) Cholesterol starvation induces differentiation

13   of the intestinal parasite Giardia lamblia. *Proc Natl Acad Sci U S A* 93(15):7628-7633.

14   17.   Lujan HD, Mowatt MR, & Nash TE (1997) Mechanisms of Giardia lamblia differentiation into

15   cysts. *Microbiol Mol Biol Rev* 61(3):294-304.

16   18.   Lujan HD, Mowatt MR, & Nash TE (1998) The molecular mechanisms of Giardia encystation.

17   *Parasitology Today* 14(11):446-450.

18   19.   Gillin FD, Boucher SE, & Reiner DS (1987) Stimulation of In-Vitro Encystation of Giardia-Lamblia

19   by Small Intestinal Conditions. *Clinical Research* 35(3):475A.

20   20.   Gillin FD, Reiner DS, & Boucher SE (1988) Small-intestinal factors promote encystation of

21   Giardia lamblia in vitro. *Infection and immunity* 56(3):705-707.

1   21.   Roxstrom-Lindquist K, Palm D, Reiner D, Ringqvist E, & Svard SG (2006) Giardia immunity--an

2   update. *Trends Parasitol* 22(1):26-31.

3   22.   Faso C, Bischof S, & Hehl AB (2013) The proteome landscape of Giardia lamblia encystation.

4   *PloS one* 8(12):e83207.

5   23.   Morf L, *et al.* (2010) The transcriptional response to encystation stimuli in Giardia lamblia is

6   restricted to a small set of genes. *Eukaryot Cell* 9(10):1566-1576.

7   24.   Sulemana A, Paget TA, & Jarroll EL (2014) Commitment to cyst formation in Giardia.

8   *Microbiology* 160(Pt 2):330-339.

9   25.   Troeger H, *et al.* (2007) Effect of chronic Giardia lamblia infection on epithelial transport and

10   barrier function in human duodenum. *Gut* 56:328-335.

11 26.   Tako EA, Hassimi MF, Li E, & Singer SM (2013) Transcriptomic analysis of the host response to

12   Giardia duodenalis infection reveals redundant mechanisms for parasite control. *MBio*

13   4(6):e00660-00613.

14 27.   Buret AG (2007) Mechanisms of epithelial dysfunction in giardiasis. *Gut* 56(3):316-317.

15 28.   Byrd LG, Conrad JT, & Nash TE (1994) Giardia lamblia infections in adult mice. *Infection and*

16   *immunity* 62(8):3583-3585.

17 29.   Singer SM (2016) Control of Giardiasis by Interleukin-17 in Humans and Mice--Are the

18   Questions All Answered? *Clin Vaccine Immunol* 23(1):2-5.

19 30.   Mayrhofer G, *et al.* (1992) The use of suckling mice to isolate and grow Giardia from

20   mammalian faecal specimens for genetic analysis. *Parasitology* 105 (Pt 2):255-263.

21 31.   Rivero FD, *et al.* (2010) Disruption of antigenic variation is crucial for effective parasite vaccine.

22   *Nature medicine* 16(5):551-557, 551p following 557.

1 32. Aggarwal A & Nash TE (1987) Comparison of two antigenically distinct Giardia lamblia isolates in

2   gerbils. *Am J Trop Med Hyg* 36(2):325-332.

3 33. Miyamoto Y & Eckmann L (2015) Drug Development Against the Major Diarrhea-Causing

4   Parasites of the Small Intestine, Cryptosporidium and Giardia. *Front Microbiol* 6:1208.

5 34. Hutchens M & Luker GD (2007) Applications of bioluminescence imaging to the study of

6   infectious diseases. *Cellular microbiology* 9(10):2315-2322.

7 35. Andreu N, Zelmer A, & Wiles S (2011) Noninvasive biophotonic imaging for studies of infectious

8   disease. *FEMS microbiology reviews* 35(2):360-394.

9 36. Wiles S, Pickard KM, Peng K, MacDonald TT, & Frankel G (2006) In vivo bioluminescence

10   imaging of the murine pathogen Citrobacter rodentium. *Infection and immunity* 74(9):5391-

11   5396.

12 37. Rhee KJ, *et al.* (2011) Determination of spatial and temporal colonization of enteropathogenic

13   E. coli and enterohemorrhagic E. coli in mice using bioluminescent in vivo imaging. *Gut*

14   *microbes* 2(1):34-41.

15 38. Gourguechon S & Cande WZ (2011) Rapid tagging and integration of genes in Giardia

16   intestinalis. *Eukaryotic Cell* 10(1):142-145.

17 39. Luo J, Lin AH, Masliah E, & Wyss-Coray T (2006) Bioluminescence imaging of Smad signaling in

18   living mice shows correlation with excitotoxic neurodegeneration. *Proc Natl Acad Sci U S A*

19   103(48):18326-18331.

20 40. Welsh DK & Kay SA (2005) Bioluminescence imaging in living organisms. *Current opinion in*

21   *biotechnology* 16(1):73-78.

1 41. Weissleder R & Ntziachristos V (2003) Shedding light onto live molecular targets. *Nature*

2 *medicine* 9(1):123-128.

3 42. Reimao JQ, *et al.* (2013) Parasite burden in Leishmania (Leishmania) amazonensis-infected

4 mice: validation of luciferase as a quantitative tool. *Journal of microbiological methods*

5 93(2):95-101.

6 43. Saeij JP, Boyle JP, Grigg ME, Arrizabalaga G, & Boothroyd JC (2005) Bioluminescence imaging of

7 Toxoplasma gondii infection in living mice reveals dramatic differences between strains.

8 *Infection and immunity* 73(2):695-702.

9 44. D'Archivio S, *et al.* (2013) Non-invasive in vivo study of the Trypanosoma vivax infectious

10 process consolidates the brain commitment in late infections. *PLoS Negl Trop Dis* 7(1):e1976.

11 45. Wampfler PB, Faso C, & Hehl AB (2014) The Cre/loxP system in Giardia lamblia: genetic

12 manipulations in a binucleate tetraploid protozoan. *Int J Parasitol*.

13 46. Ringqvist E, Avesson L, Söderbom F, & Svärd SG (2011) Transcriptional changes in Giardia during

14 host-parasite interactions. *International journal for parasitology* 41:277-285.

15 47. Einarsson E, *et al.* (2016) Coordinated Changes in Gene Expression Throughout Encystation of

16 Giardia intestinalis. *PLoS Negl Trop Dis* 10(3):e0004571.

17 48. Morrison HG, *et al.* (2007) Genomic minimalism in the early diverging intestinal parasite *Giardia*

18 *lamblia*. *Science* 317(5846):1921-1926.

19 49. Hehl AB, Marti M, & Kohler P (2000) Stage-specific expression and targeting of cyst wall

20 protein-green fluorescent protein chimeras in Giardia. *Mol Biol Cell* 11(5):1789-1800.

1   50.   Lujan HD, Mowatt MR, Conrad JT, Bowers B, & Nash TE (1995) Identification of a novel Giardia

2   lamblia cyst wall protein with leucine-rich repeats. Implications for secretory granule formation

3   and protein assembly into the cyst wall. *J Biol Chem* 270(49):29307-29313.

4   51.   Boucher SEM & Gillin FD (1990) Excystation of in vitro-derived Giardia lamblia cysts. *Infection*

5   *and immunity* 58(11):3516-3522.

6   52.   Ansell BR, *et al.* (2015) Drug resistance in Giardia duodenalis. *Biotechnol Adv* 33(6 Pt 1):888-

7   901.

8   53.   Leitsch D (2015) Drug Resistance in the Microaerophilic Parasite. *Curr Trop Med Rep* 2(3):128-

9   135.

10 54.   Solaymani-Mohammadi S & Singer SM (2011) Host immunity and pathogen strain contribute to

11   intestinal disaccharidase impairment following gut infection. *J Immunol* 187(7):3769-3775.

12 55.   Barbara J. Davids aFDG (2011) Methods for Giardia culture, cryopreservation, encystation, and

13   excystation in vitro. *Giardia: A Model Organism*, ed Lujan HaS, S. (Springer Verlag, New York,

14   NY), pp 381-394.

15 56.   Singer SM & Nash TE (2000) T-cell-dependent control of acute Giardia lamblia infections in

16   mice. *Infection and immunity* 68(1):170-175.

17 57.   Foucault ML, Thomas L, Goussard S, Branchini BR, & Grillot-Courvalin C (2010) In vivo

18   bioluminescence imaging for the study of intestinal colonization by Escherichia coli in mice.

19   *Appl Environ Microbiol* 76(1):264-274.

20 58.   Belosevic AM, Faubert GM, Maclean JD, Law C, & Croll NA (1983) Giardia lamblia Infections in

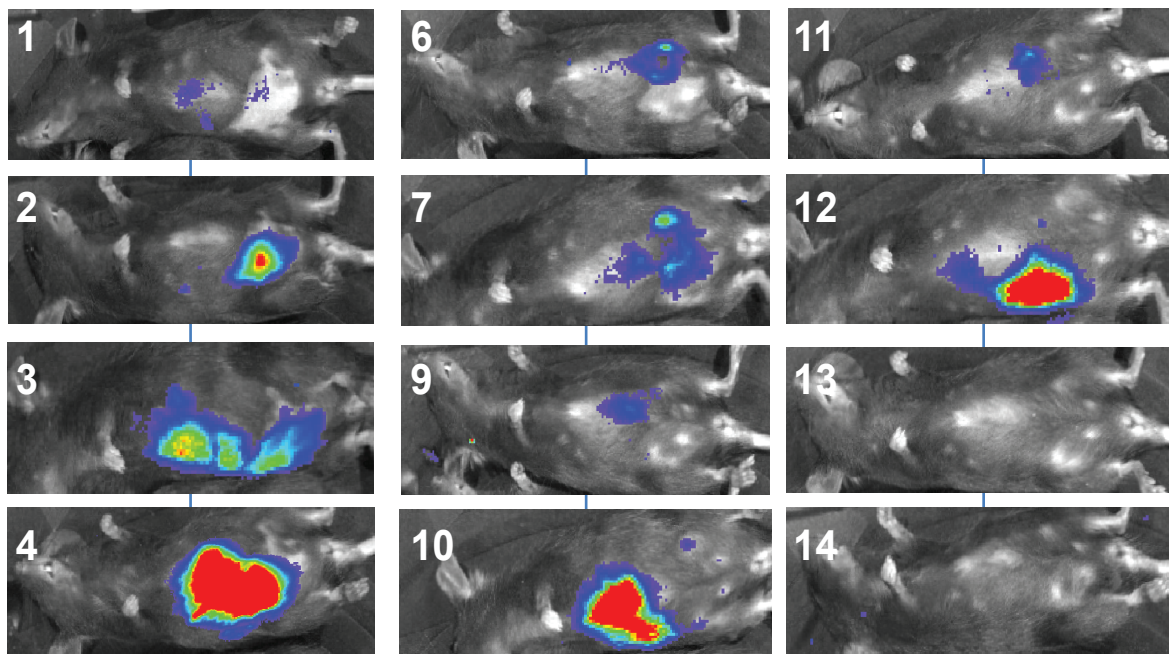21   Mongolian Gerbils : An Animal Model. 147:222-226.

1 59.   Araujo NS, *et al.* (2008) Giardia duodenalis: pathological alterations in gerbils, Meriones

2   unguiculatus, infected with different dosages of trophozoites. *Exp Parasitol* 118(4):449-457.

3 60.   Watkins RR & Eckmann L (2014) Treatment of giardiasis: current status and future directions.

4   *Current infectious disease reports* 16(2):396.

5 61.   Gillin FD, *et al.* (1987) Encystation and expression of cyst antigens by Giardia lamblia in vitro.

6   *Science* 235(4792):1040-1043.

7 62.   Owen RL, Nemanic PC, & Stevens DP (1979) Ultrastructural observations on giardiasis in a

8   murine model. I. Intestinal distribution, attachment, and relationship to the immune system of

9   Giardia muris. *Gastroenterology* 76(4):757-769.

10 63. Bowcutt R, *et al.* (2014) Heterogeneity across the murine small and large intestine. *World

11   journal of gastroenterology : WJG* 20(41):15216-15232.

12 64. Portugal S, *et al.* (2011) Host-mediated regulation of superinfection in malaria. *Nature medicine*

13   17(6):732-737.

14 65. Matthews KR, McCulloch R, & Morrison LJ (2015) The within-host dynamics of African

15   trypanosome infections. *Philos Trans R Soc Lond B Biol Sci* 370(1675).

16 66. Mony BM, *et al.* (2014) Genome-wide dissection of the quorum sensing signalling pathway in

17   Trypanosoma brucei. *Nature* 505(7485):681-685.

18 67. Loomis WF (2014) Cell signaling during development of Dictyostelium. *Dev Biol* 391(1):1-16.

19 68. Mandal J & Parija SC (2013) Ethics of involving animals in research. *Tropical parasitology* 3(1):4-

20   6.

21 69. Branchini BR, *et al.* (2007) Thermostable red and green light-producing firefly luciferase

22   mutants for bioluminescent reporter applications. *Analytical biochemistry* 361(2):253-262.

1 70. Cevenini L, *et al.* (2014) Multicolor bioluminescence boosts malaria research: quantitative dual-

2 color assay and single-cell imaging in Plasmodium falciparum parasites. *Analytical chemistry*

3 86(17):8814-8821.

4 71. Maguire CA, *et al.* (2013) Triple bioluminescence imaging for in vivo monitoring of cellular

5 processes. *Molecular therapy. Nucleic acids* 2:e99.

6 72. Tejman-Yarden N & Eckmann L (2011) New approaches to the treatment of giardiasis. *Curr Opin*

7 *Infect Dis* 24(5):451-456.

8 73. Gourguechon S, Holt LJ, & Cande WZ (2013) The Giardia cell cycle progresses independently of

9 the anaphase-promoting complex. *Journal of cell science* 126(Pt 10):2246-2255.

10 74. Li L & Wang CC (2006) A likely molecular basis of the susceptibility of Giardia lamblia towards

11 oxygen. *Molecular microbiology* 59(1):202-211.

12 75. Frank DN, *et al.* (2011) Disease phenotype and genotype are associated with shifts in intestinal-

13 associated microbiota in inflammatory bowel diseases. *Inflamm Bowel Dis* 17(1):179-184.

14 76. Merino MC, Zamponi N, Vranych CV, Touz MC, & Ropolo AS (2014) Identification of Giardia

15 lamblia DHHC proteins and the role of protein S-palmitoylation in the encystation process. *PLoS*

16 *Negl Trop Dis* 8(7):e2997.

17 77. Sagolla MS, Dawson SC, Mancuso JJ, & Cande WZ (2006) Three-dimensional analysis of mitosis

18 and cytokinesis in the binucleate parasite Giardia intestinalis. *Journal of cell science* 119(Pt
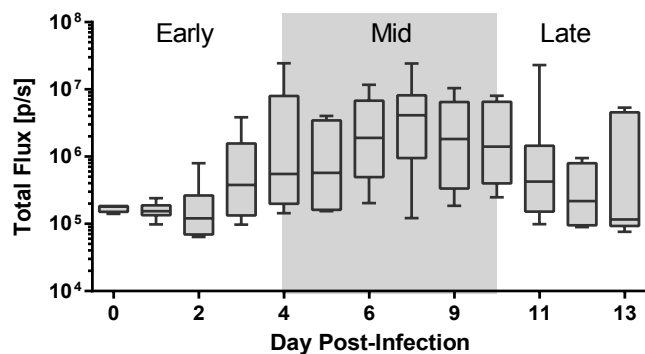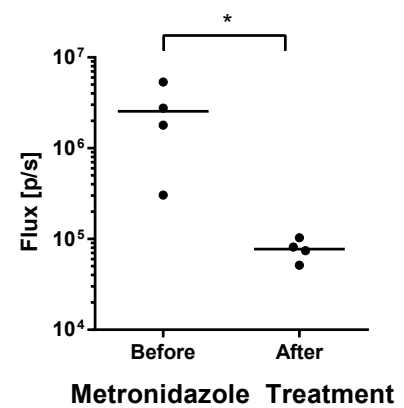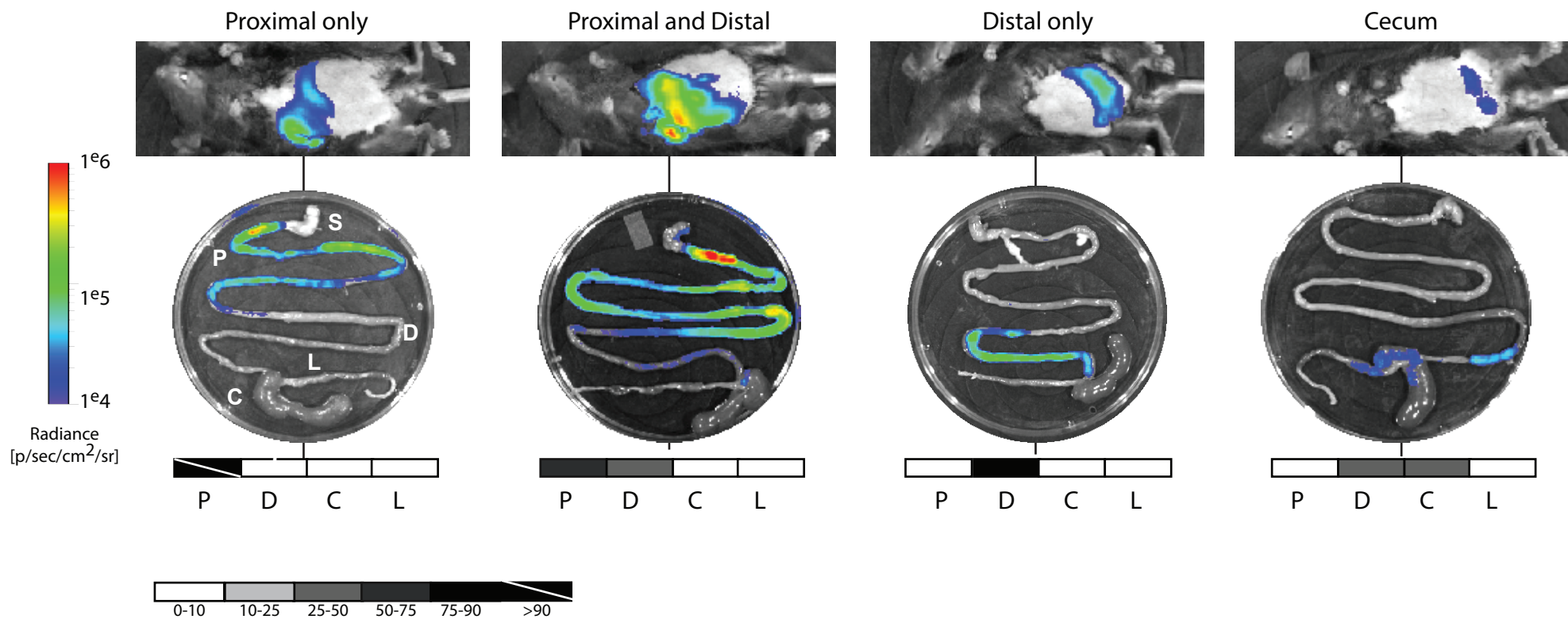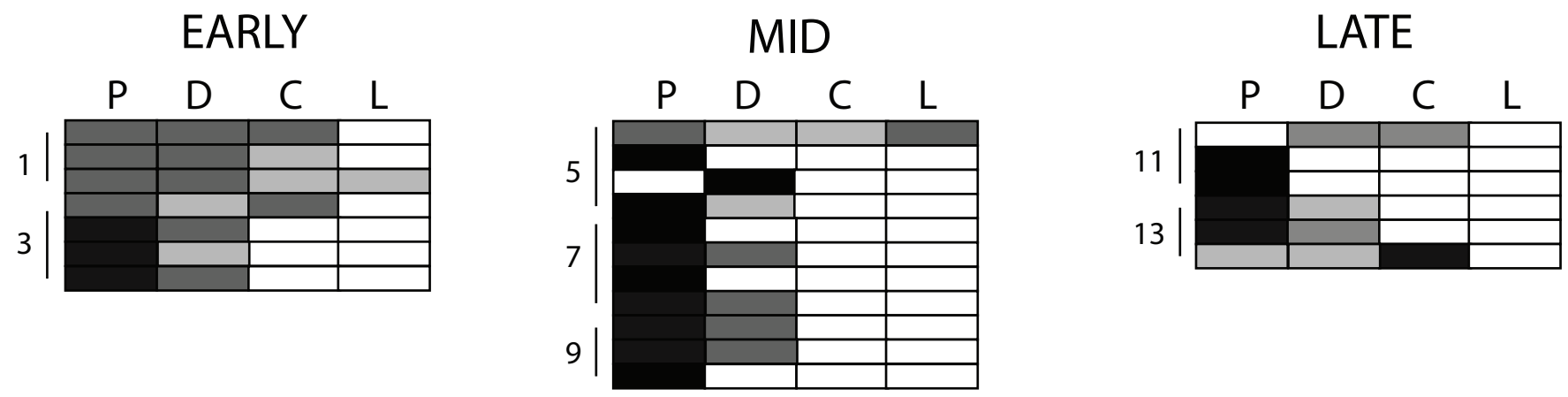
19 23):4889-4900.

20

A

Proximal only | Proximal and Distal | Distal only | Cecum

Radiance [p/sec/cm²/sr]

0-10　10-25　25-50　50-75　75-90　>90

B

EARLY　　　MID　　　LATE